



Frequency Conversion of Optical Vortex Arrays Through Four-Wave Mixing in Hot Atomic Gases

L. A. Mendoza-López, J. G. Acosta-Montes, J. A. Bernal-Orozco, Y. M. Torres, N. Arias-Téllez, R. Jáuregui* and D. Sahagún Sánchez*

Departamento de Física Cuántica y Fotónica, Instituto de Física, Circuito de la Investigación Científica s/n, Universidad Nacional Autónoma de México, Ciudad Universitaria, Ciudad de México, México

OPEN ACCESS

Edited by:

Mario Alan Quiroz-Juarez,
Autonomous Metropolitan University,
Mexico

Reviewed by:

Jietai Jing,
East China Normal University, China
Jianming Wen,
Kennesaw State University,
United States

*Correspondence:

R. Jáuregui
rocio@fisica.unam.mx
D. Sahagún Sánchez
sahagun@fisica.unam.mx

Specialty section:

This article was submitted to
Quantum Engineering and
Technology,
a section of the journal
Frontiers in Physics

Received: 12 March 2022

Accepted: 16 May 2022

Published: 11 July 2022

Citation:

Mendoza-López LA, Acosta-Montes JG, Bernal-Orozco JA, Torres YM, Arias-Téllez N, Jáuregui R and Sánchez DS (2022) Frequency Conversion of Optical Vortex Arrays Through Four-Wave Mixing in Hot Atomic Gases. *Front. Phys.* 10:895023. doi: 10.3389/fphy.2022.895023

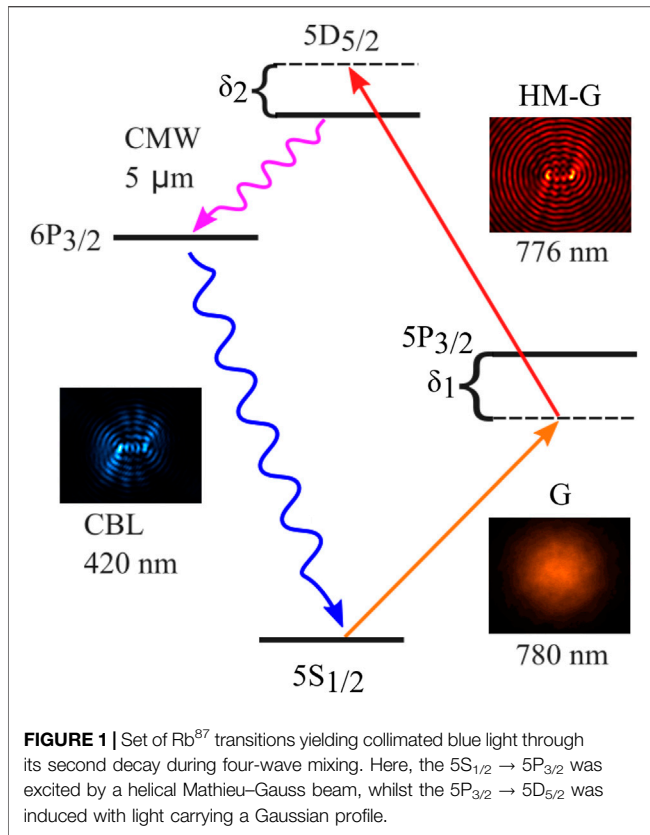
Arrays of multiple vortices were transferred from infrared to the blue region of the optical spectrum. This demonstration was achieved by inducing four-wave mixing in an atomic gas with a Gaussian beam and a quasi-invariant propagation beam of the Mathieu type. The latter structure was analyzed in the Fourier space for the pump and the generated light. In both cases, the phase structure can be written with a compact mathematical expression by using the same parameters within experimental error bars. A Michelson–Morley interferometer was used to confirm that a phase singularity was present at each site as predicted by the theory. These studies add to the available control over orbital angular momentum in photons generated by atoms, which has a broad span of applications in quantum and classical information management.

Keywords: four-wave mixing, atomic gases, quantum light, structured beams, orbital angular momentum, hot atoms, Mathieu beams, up-conversion

1 INTRODUCTION

The angular momentum of light has been the subject of fundamental discussions about its analogies with atomic variables for nearly one century [1]. In 1993, Beijersbergen and colleagues demonstrated that, indeed, laser light can carry orbital angular momentum (OAM) by means of an appropriate preparation [2]. Thereafter, the OAM of light has been employed for a vast quantity of classical applications covering from microscopy and micro-manipulation to astrophysics and medicine [3]. This variable became an additional resource of quantum engineering once researchers were able to transfer it to correlated photons through spontaneous parametric down conversion (SPDC) [4, 5]; large Hilbert spaces became available for the subsequent treatment of entangled-photon pairs [6–8].

Since OAM can be transferred to and retrieved from atoms [9], it is also possible to generate quantum light-carrying OAM by inducing four-wave mixing (FWM). Controlling the electromagnetic degrees of freedom through this non-linear process makes it possible to generate light correlated in the time [10], useful to build, for example, quantum memories [11]. Ladder-type schemes of FWM in the alkali elements allow to convert light from one end to the other end of the optical spectrum, and even beyond. For example, exciting applications arose from generating and detecting electromagnetic fields at terahertz frequencies through FWM [12–15]. Here, we drive attention to the double transition $5S_{1/2} \rightarrow 5P_{3/2} \rightarrow 5D_{5/2}$ of Rb^{87} , which yields a beam at 420 nm during the second step of its cascade decay that can be readily detected [12] (**Figure 1**). This scheme has been a workhorse to those interested in developing the usage of OAM on light with atomic origin because the up-converted beam is relatively simple to collimate and optimize in setups where FWM is induced on hot atoms [16, 17]. Thus, the experiments involving this collimated blue



light (CBL) are suitable for building scalable and robust devices, as desirable for practical applications. Quantum technologies are included since phase matching during the FWM process indicates that the OAM entanglement should be present between the CBL and the electromagnetic field at $5 \mu\text{m}$ (CMW), emitted during the cascade decay, whenever the appropriate choice in the parameters of the pump beams is carried out, especially if the total topological charge of the pump beams is large enough [18].

Single, optical vortices were first up-converted by [19]. In [20], it was shown that it is possible to perform arithmetic operations with the OAM traveling on both pump beams through FWM. Moreover, optical vortices with a helicity up to ± 30 are transferable to the CBL as well [21]. In those experiments, the FWM process was pumped with Laguerre–Gauss beams that carry one phase singularity along a straight dislocation line. However, since 2002, it has been possible to generate arrays of optical vortices on laser light using Mathieu modes [22], members of the quasi-propagation invariant beam family [23]. This family of structured beams has given birth to numerous scientific discoveries through micro-manipulation of biological materials [see for example [24]]. More recently, they have yielded new methods to control the spatial and the correlation properties of photon pairs generated by SPDC [25].

In a recent publication, we reported the up-conversion of quasi-propagation invariant Mathieu beams through an FWM process in hot atoms [26]. There, the light-mode analysis was performed by studying in detail the Fourier

and configuration spaces of the electromagnetic fields. These are well-established methods for experiments using non-linear crystals. However, they were introduced to the context of atomic gases in [26]. For those experiments neither the pump beams nor the CBL exhibited vortices. In this article, we report that modes containing arrays of optical vortices are also inherited *via* FWM. We also show that Michelson–Morley interferometry is a suitable tool to confirm this fact. A simulation of the classical interference pattern serves as a reference to locate the phase singularities. We induced FWM as depicted in **Figure 1**: with a Gaussian beam (G) resonant to the $5S_{1/2} \rightarrow 5P_{3/2}$ transition and a helical Mathieu–Gauss beam (HM-G) exciting the $5P_{3/2} \rightarrow 5D_{5/2}$ second step. We demonstrated that a non-trivial density of OAM was transferred from the pumping HM-G beam to the generated CBL. Our findings complement studies of non-linear processes, where the local density of angular momentum of light is connected to a spatially dependent polarization [27]. The results that we present here add two tools to experiments of this kind: conversion of light with a quasi-propagation invariant structure and several dislocation lines; and an extraordinary control over the properties of the generated light based on manipulating the atomic states involved in the non-linear process.

2 HELICAL MATHIEU BEAMS

In this section, we describe a few basic features of the structured light fields used in the experiment. We start with the elementary Mathieu modes that do not exhibit vortices but are the basis from which helical Mathieu beams—which may have more than one dislocation line—are built.

Elementary Mathieu modes are written in terms of scalar functions $\Psi(\vec{r}, t)$ that solve the following wave equation:

$$\left[\nabla^2 - \frac{1}{c^2} \frac{\partial^2}{\partial t^2} \right] \Psi(\vec{r}, t) = 0, \quad (1)$$

in elliptic-cylindrical coordinates $\{\xi, \eta, z\}$. These coordinates are related to the Cartesian space $\{x, y, z\}$ by the transformations:

$$x + iy = h \cosh(\xi + i\eta), \quad \xi \in [0, \infty), \quad \eta \in [0, 2\pi); \quad \text{and} \quad z = z, \quad (2)$$

where the constant h corresponds to half the inter-focal distance of the ellipses defining the coordinate system. The wave-equation in elliptic-cylindrical coordinates can be solved by the separation of variable method. By demanding the solutions to have a well-defined parity with respect to reflections through the z -plane, and to take finite value as $\xi \rightarrow \infty$, the following expressions for the scalar wave function $\Psi(\vec{r}, t)$ are found [28]:

$$\begin{aligned} \Psi_{\kappa}^{(e)}(\vec{r}, t) &= A_{\kappa} \text{Ie}_{\kappa}(\xi, q) \text{ce}_{\kappa}(\eta, q) e^{i(k_z z - \omega t)}, \\ \Psi_{\kappa}^{(o)}(\vec{r}, t) &= B_{\kappa} \text{Jo}_{\kappa}(\xi, q) \text{se}_{\kappa}(\eta, q) e^{i(k_z z - \omega t)}. \end{aligned} \quad (3)$$

Here, $\text{ce}_{\kappa}(\eta, q)$ and $\text{se}_{\kappa}(\eta, q)$ are the real even and odd ordinary solutions of the Mathieu equation:

$$\left[\frac{d^2}{d\eta^2} + a_n - 2q \cos 2\eta \right] f_n^{(p)}(\eta, q) = 0, \quad q = \left(\frac{h\kappa_\perp}{2} \right)^2, \quad (4)$$

$$\kappa_\perp^2 = (\omega/c)^2 - k_z^2;$$

and $Je_n(\eta, q)$ and $Jo_n(\eta, q)$ solve its modified analog as follows:

$$\left[\frac{d^2}{d\xi^2} + a_n - 2q \cosh 2\xi \right] F_n^{(p)}(\xi, q) = 0. \quad (5)$$

In general, the characteristic values a_n and b_n , for even and odd Mathieu functions, respectively, are ordered by the progressive parameter n . For a given n , $a_n \neq b_n$. The label κ in **Eq. 3** denotes a set of separation constants ω, k_z, n .

The wave function $\Psi(\vec{r}, t)$ satisfies the following eigenvalue equations [29],

$$i \frac{\partial}{\partial t} \Psi(\vec{r}, t) = \omega \Psi(\vec{r}, t), \quad -i \frac{\partial}{\partial z} \Psi(\vec{r}, t) = k_z \Psi(\vec{r}, t), \quad (6a)$$

$$\frac{1}{2} \left[\left(\hat{l}_+ \right)_z \left(\hat{l}_- \right)_z + \left(\hat{l}_- \right)_z \left(\hat{l}_+ \right)_z \right] \Psi(\vec{r}, t) = a_n \Psi(\vec{r}, t),$$

$$\hat{l}_\pm = (\vec{r} - (0, 0, \pm h)) \times (-i\vec{\nabla}); \quad (6b)$$

$(\hat{l}_\pm)_z$ is the z-component of the \hat{l}_\pm vector.

As a consequence, once the generalization to vectorial electromagnetic waves is carried out and the standard quantization is performed [30], in the quantum realm, the parameters $\{\omega, k_z, a_n\}$ are assigned to a photon described by these EM modes, an energy $\hbar\omega$, a linear momentum along the main propagation axis $\hbar k_z$, and an algebraic mean value of the z-component of the angular momentum with respect to the axis passing through the foci of the elliptic coordinate system, $\hbar^2 a_n$.

The angular spectrum of Mathieu fields,

$$S_n^{(p)}(\theta_{\vec{k}}, \varphi_{\vec{k}}; a, q) = f_n^{(p)}(\varphi_{\vec{k}}, q) \delta\left(\sin \theta_{\vec{k}} - \kappa_\perp c / \omega\right) \frac{|\cos \theta_{\vec{k}}|}{\sin \theta_{\vec{k}}}, \quad (7)$$

allows them to be written as the superposition of plane waves,

$$\Psi^{(p)}(\vec{r}, t) = \int d\omega \alpha(\omega) \int d^3k \delta(\omega - c|\vec{k}|) e^{i\vec{k}\cdot\vec{r} - i\omega t} S^{(p)}(\theta_{\vec{k}}, \varphi_{\vec{k}}). \quad (8)$$

The delta factor in **Eq. 7** guarantees cylindrical symmetry on the field by restricting the participating plane waves to those sharing a common modulus κ_\perp of their transverse wave vector. Nevertheless, actual realizations of Mathieu beams involve a conic-shell volume within the wave-vector space derived from replacing the delta distribution by a properly normalized Gaussian distribution [31]:

$$\delta(\sin \theta - \kappa_\perp c / \omega) \rightarrow \frac{1}{(c\sigma/\omega)\sqrt{2\pi}} e^{-\frac{(\sin \theta - \kappa_\perp c / \omega)^2}{2(c\sigma/\omega)^2}} \quad (9)$$

with waist σ . This spectrum can be codified in a spatial light modulator (SLM) to generate electromagnetic Mathieu modes in the paraxial regime ($\kappa_\perp \ll |k_z|$) with a polarization determined by the quasi-plane waves that impinge the SLM. Transfer of the elementary Mathieu modes described here from infrared to blue light via FWM in atomic gases has recently been reported [26].

Optical vortices in scalar fields are locations where the phase is not well defined and exhibits a change of $2m\phi$ along any closed loop around them; the integer m is called topological charge. Close to a vortex, the field magnitude is zero, but the density of orbital angular momentum is not null. Even though the phase structure of scalar solutions $\Psi_\kappa^{(e)}(\vec{r}, t)$ and $\Psi_\kappa^{(o)}(\vec{r}, t)$ do not exhibit this kind of singularity, a proper superposition of them can give rise to one or more optical vortices with topological charges ± 1 . This happens for generalized-helical Mathieu beams with angular spectrum

$$S_\kappa^{(h)}(\theta_{\vec{k}}, \varphi_{\vec{k}}) = \mathcal{I}_n^{(e)} ce_n(\varphi_{\vec{k}}, q) + i\mathcal{I}_n^{(o)} se_n(\varphi_{\vec{k}}, q). \quad (10)$$

Most studies in the literature consider the case for which the real constants $\mathcal{I}_n^{(e)}$ and $\mathcal{I}_n^{(o)}$ have the same absolute value [32].

By varying the plane of observation, optical vortices create the so-called dislocation lines. In the ideal case ($\sigma \rightarrow 0$), helical Mathieu beams are propagation invariant, and the dislocation lines are straight and parallel to the main direction of propagation. For actual helical Mathieu–Gauss beams, the dislocation lines are open but exhibit a slight curvature due to the unavoidable partial focusing of any Gaussian-like beam.

For the experiments reported here, we used a helical Mathieu–Gauss mode with $n = 4$, $\mathcal{I}_n^{(e)} = \mathcal{I}_n^{(o)}$, $\kappa_\perp = 11 \text{ mm}^{-1}$, $\sigma = 0.038\kappa_\perp$, and $q = 21.78$ as an illustrative example. A simulation of its intensity profile on the $z = 0$ plane is shown in **Figure 2A**; some vortices are highlighted with blue circles where the intensity is null. The corresponding phase diagram is shown in **Figure 2A**. There, one can corroborate that the phase changes by 2π around the neighborhood highlighted in (A), so that the topological charge is unitary. **Figures 2C,D** show this beam in the Fourier space. **Figure 2C** depicts its intensity in the $k_x - k_y$ plane, and **Figure 2D** plots its angular dependence along the central κ_\perp circle.

2.1 Phase-Matching Conditions Involving Gaussian and Helical Mathieu–Gaussian Pump Beams in FWM

Our experiment concerns the four-wave mixing process illustrated in **Figure 1**, where the $5D_{5/2}$ state of Rb^{87} is populated through a ladder transition excited by G and HM-G. Both pump beams satisfy the paraxial condition $k_z \sim \omega/c$. The cascade route explored in this work involves an electric-dipole decay in the microwave region, $5D_{5/2} \rightarrow 6P_{3/2}$, and a blue photon arising from the $6P_{3/2} \rightarrow 5S_{1/2}$ relaxation. A standard perturbative analysis of the steady-state amplitude for spontaneous emission of microwaves with electric fields $\vec{E}_{CMW}(\vec{r})e^{-i\omega_{CMW}t}$ and blue photons with $\vec{E}_{CBL}^*(\vec{r})e^{-i\omega_{CBL}t}$ shows that it is proportional to

$$\mathfrak{F}[\vec{E}_{CMW}, \vec{E}_{CBL}] = \int_{-\infty}^{\infty} dt e^{i(\omega_{CMW} + \omega_{CBL})t} \int d^3r \vec{d}_{CMW}^* \cdot \vec{E}_{CMW}^*(\vec{r}) \vec{d}_{CBL}^* \cdot \vec{E}_{CBL}^*(\vec{r}) \Omega_G(\vec{r}, t) \Omega_{HM-G}(\vec{r}, t) f_A(\vec{r}, t), \quad (11)$$

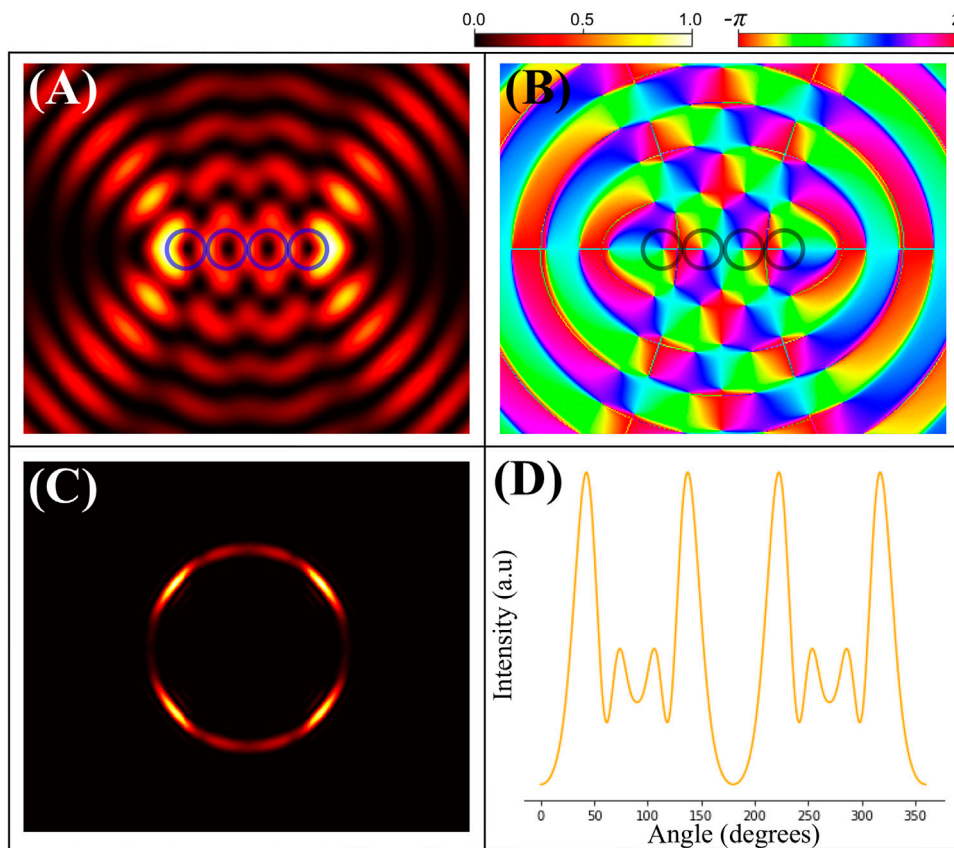


FIGURE 2 | Plots simulating a helical Mathieu–Gauss beam of order 4 (chosen to prepare HM-G). **(A)** Intensity profile; **(B)** spatial dependency of its phase. The blue circles on **(A)** and **(B)** enclose zero-field regions where optical vortices are expected. **(C)** Fourier ring formed at the focal length of the lens used for its experimental manipulation, and the orange curve in **(D)** illustrates the corresponding angular spectrum.

where \vec{d}_{CMW} (\vec{d}_{CBL}) is the dipole moment of the $5D_{5/2} \rightarrow 6P_{3/2}$ ($6P_{3/2} \rightarrow 5S_{3/2}$) atomic transition and $f_A(\vec{r}, t)$ is the atomic density; the Rabi frequencies of the pump beams, $\Omega_G(\vec{r}, t)$ and $\Omega_{HM-G}(\vec{r}, t)$, encode their space-time structure. For ideal monochromatic G and HM-G, the temporal integral yields the phase matching condition

$$\omega_G + \omega_{HM-G} = \omega_{CML} + \omega_{CBL} \quad (12)$$

with angular frequency ω_{CML} (ω_{CBL}) in the microwave (blue) region. Meanwhile, integration over the z -coordinate and the paraxial approximation gives rise to

$$(\mathbf{k}_G)_z + (\mathbf{k}_{HM-G})_z = (\mathbf{k}_{CML})_z + (\mathbf{k}_{CBL})_z. \quad (13)$$

As in [26], the transverse structure of G is a superposition of plane waves with $|\vec{k}_\perp|$ centered at zero and the transverse structure of HM-G centered at $|\vec{k}_\perp|$ with a finite value. Photons of CBL have a wider wave-vector range than the microwaves, and thus, it may inherit the k_\perp structure of HM-G. Consequently, the down-converted modes are expected to have a Gaussian-like transverse configuration. An important difference with experiments reported in [26] is the possibility that the *local* phase structure of the vortices could have been transferred to

both CBL and CML. That may happen to photons in the vicinity of a phase singularity with a topological charge m since the Rabi frequency $\Omega_{HM-G}(r, t)$ is position-dependent. In such case, the $E_{CML}^z(\vec{r})$ and $E_{CBL}^z(\vec{r})$ electric fields exhibit a phase singularity where their topological charges m_{CBL} and m_{CML} satisfy

$$m_{HM-G} = m_{CMW} + m_{CBL}, \quad (14)$$

maximizing the integration of $|\Im[\vec{E}_{CMW}, \vec{E}_{CBL}]|$ in a neighborhood around each phase singularity of $\Omega_{HM-G}(\vec{r}, t)$.

Since for Mathieu beams, the absolute value of the topological charge is either 1 or 0 (absence of phase singularity), it is expected that the phase singularities of the CBL light should add to either ± 1 or zero. If $|m_{CBL}| > 1$, its complement would require a topological charge of even greater absolute value $|m_{CMW}| > |m_{CBL}|$ to guarantee the local phase-matching. Thus, dislocation lines in the pump, in the up-converted photons, and in the down-converted photons could evolve complex enough to compromise their stability. In a simpler scheme, vortices with a topological charge equal to that of the pump, Mathieu beams are transferred to the blue light. This is congruent with Ref. [26], where the Mathieu structure of even and odd modes is directly transferred to the CBL beam. It also extends to a local-space context, the

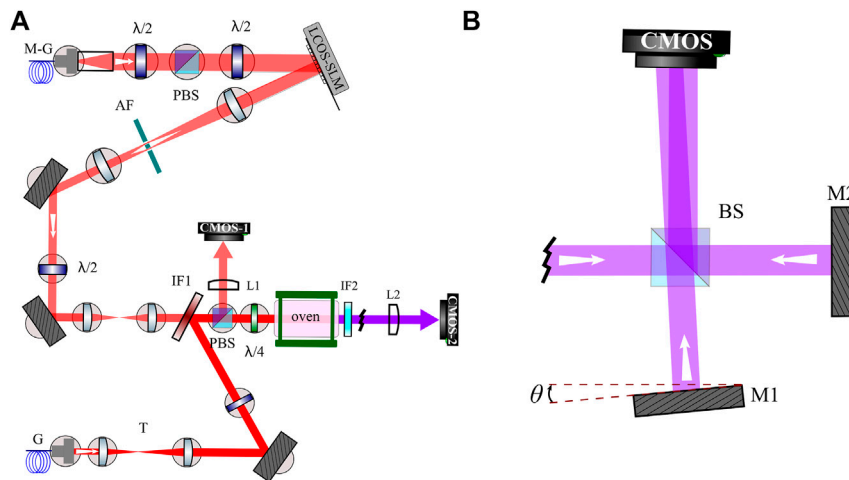


FIGURE 3 | Experimental setup to induce FWM in a hot atomic vapor of Rb^{87} with one helical Mathieu–Gauss (top) and a Gaussian beam (bottom). **(A)** Both pump beams are prepared and overlapped through the atomic sample whilst being heated by an oven. **(B)** Michelson–Morley interferometer that replaces the Fourier and configuration analysis setup for locating the optical vortices.

discussion presented in [18], which predicts that the topological charge of Laguerre–Gauss beams will preferably be transferred to the blue light for paraxial-pump beams satisfying the Boyd condition, unless the topological charge of those pump beams is large enough.

3 EXPERIMENT

To perform experiments, we used a similar apparatus as that reported in [26] with an additional interferometric module. Here, we describe only its main features and the Michelson–Morley arrangement by which the optical singularities were detected.

The experimental setup is schematized in **Figure 3**. Both HM-G and G pump beams are frequency-stabilized in separate spectroscopy setups which are not shown. Every data reported in this article were taken with G resonant to the $5S_{1/2} \rightarrow 5P_{3/2}$ transition ($\delta_1 = 0$); δ_2 was set to -16.2 MHz, optimizing the intensity of CBL on its Fourier plane within a ± 20 MHz range. The top part of **Figure 3A** illustrates the optical arrangement for generating arbitrary Mathieu–Gauss beams with a phase-only SLM [33]. Their cross section has a long diameter of about 4 mm. This size is matched to the G beam with the help of telescope T1, as shown in the bottom part of **Figure 3A**. Experiments were performed by saturating the first FWM step with a power of 27 mW on G; HM-G carried 7 mW only. Both beams are overlapped on an interference filter F1 to co-propagate them across a heated spectroscopy cell. This guarantees the Boyd criteria for the efficiency in the FWM process. The Fourier space of HM-G is imaged right before interacting with atoms by placing CMOS-I at the focal plane of lens L1. The CBL is equally monitored by focusing it with L2 on CMOS-2.

Figure 3B depicts the Michelson–Morley module added to analyze the phase of CBL. This interferometer is a variation of the simplest technique to detect an optical vortex: to interfere with

the studied beam with an inclined plane wave, resulting in a fork-like interferogram. By counting the fork number in the resulting pattern and observing their relative orientation, the vortex order and its corresponding sign can be precisely assigned. We did not try to produce a blue plane wave to interfere with CBL because that requires an extra laser. Instead, we split the CBL, letting it to interfere with itself. Clear inference patterns can be readily observed by overlapping the center of one arm with the external field of the other, where the CBL-phase structure has its smallest variations [34].

The Michelson–Morley module is placed instead of lens L2 and CMOS-2 at the right end of **Figure 3A**—right after the interference filter IF2, which removes remnants of pumping light. Two arms with CBL are created by a 50:50 beam splitter cube. Each one of them is retro-reflected by its respective mirror (M1 and M2 in **Figure 3B**) in order to overlap them on a simple CMOS camera. For this interferometer to work, the arms should be slightly misaligned. The distance between them when impinging on the CMOS chip is controlled using a translation stage driving the angle θ of M1.

4 RESULTS

We characterized both electromagnetic fields by measuring their angular spectra from images of their Fourier plane to show that the structure of HM-G is transferred to CBL through the FWM process. This allows to formulate a compact expression for the two beams in terms of parameters that define the ideal Mathieu mode programmed to the SLM [26]. The analyses were performed for the illustrative example described in **Figure 2**. Its relevant parameters are shown in **Table 1**. The interference patterns of CBL with itself confirmed that the full set of vortices, theoretically expected on the major axis of the Mathieu mode, are present in the generated light.

TABLE 1 | Consolidation of parameters measured from angular spectra of the M-G pump beam and the CBL; the parameters used for simulating the chosen illustrative mode, displayed in **Figure 2**, are shown for reference.

	SLM (theory)	HM-G	CBL
κ_{\perp} (mm ⁻¹)	11	33.0 ± 0.34	33.2 ± 0.78
$\mathcal{I}_4^{(e)}$ (a.u.)	1.00	1.00 ± 0.06	0.99 ± 0.13
$\mathcal{I}_4^{(o)}$ (a.u.)	1.00	0.98 ± 0.08	1.00 ± 0.16
q	21.78	21.4 ± 0.65	21.1 ± 1.20
ϕ_0 (degrees)	0.00	-7.70 ± 0.27	-5.38 ± 0.51

4.1 Analysis in the Fourier Space

Fourier rings of CBL were imaged for an atomic-gas temperature ranging from 70 to 120°C. The data presented in this section were taken at 95°C because this is one of temperatures for which the angular spectrum of CBL yields a visibility that allows reliable identification of the parameters that mathematically describe the generated field.

Figure 4 depicts the Fourier analysis for both G-M (A) and CBL (B). Their transverse wave-numbers are given by the radius of the averaged ring scaled by $1/f\lambda$, where f is the focal length of

the corresponding Fourier lens and λ is the wavelength of the light [35]. The measured values are $\kappa_{\perp}^{HM-G} = 33.0 \pm 0.34$ mm⁻¹ (red ring) and $\kappa_{\perp}^{CBL} = 33.2 \pm 0.78$ mm⁻¹ (blue ring); essentially, all the transverse momentum was inherited to the blue light through the FWM process, as expected. The angular spectra of both electromagnetic fields are analyzed at the right of **Figure 4**. There, blue dots are data extracted from the circle with radius κ_{\perp} for each case, and orange curves are the best fit to them with **Eq. 10**. Both graphs display a noise offset that was accounted for by adding a constant term to the adjusted function. **Table 1** shows the parameters yielding the best fit for the angular spectra of HM-G and CBL with a coefficient of reliability R^2 of 0.89 and 0.81, respectively. It is useful to first verify that $\mathcal{I}_4^{(e)} = |\mathcal{I}_4^{(o)}|$ in HM-G, as programmed with the SLM. This is indeed the case within error bars as can be read from the second column, where both values normalized by $\mathcal{I}_4^{(e)}$ are shown. The full characterization of HM-G in the wave-vector space finishes by realizing that the fitted ellipticity parameter q (21.4 ± 0.65) agrees with its programmed value in the SLM.

Evidence of an enhanced, spatial, and spectral coherence on the CBL has been observed [36]. This imposes an extra difficulty on aligning and overlapping HM-G with G to

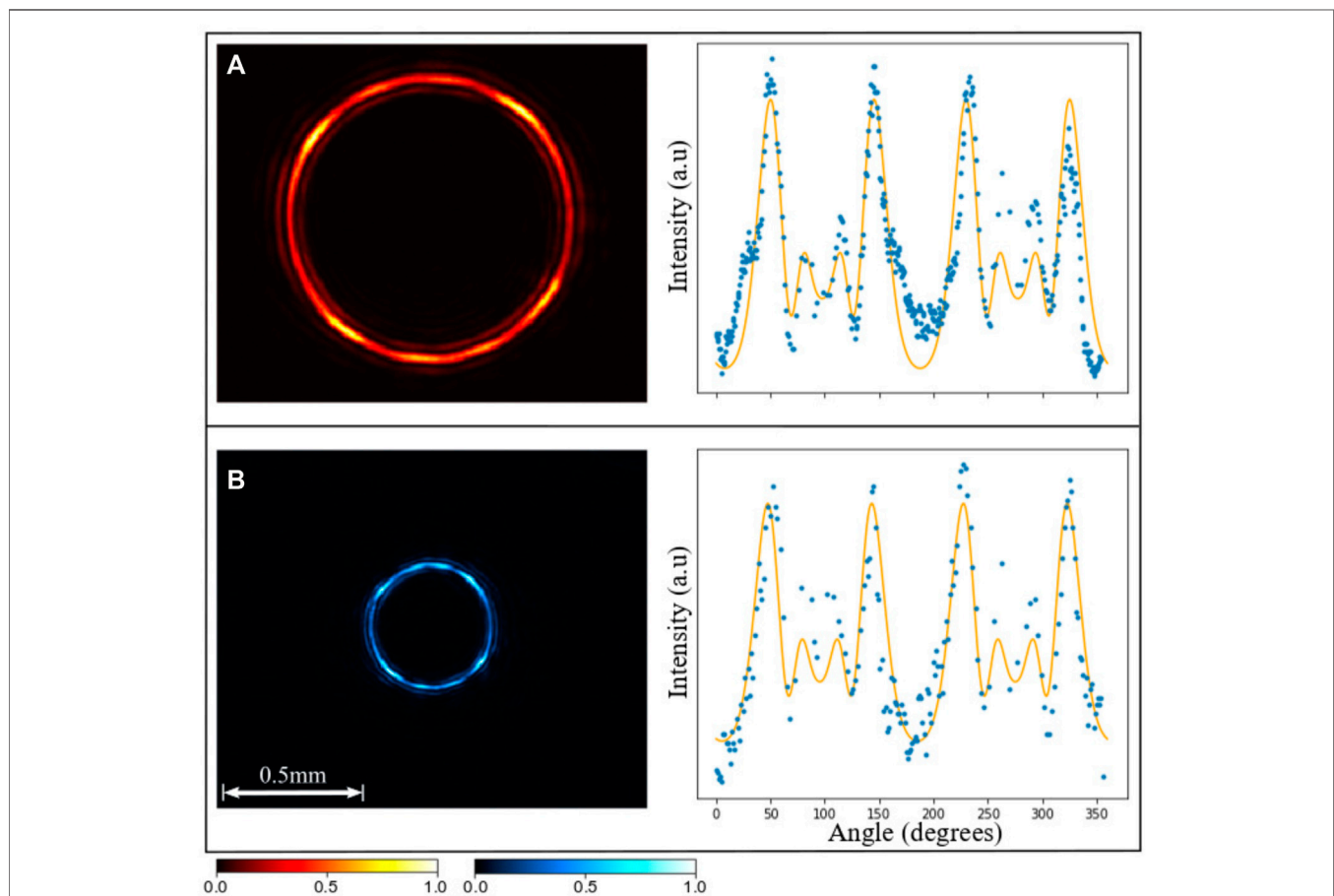
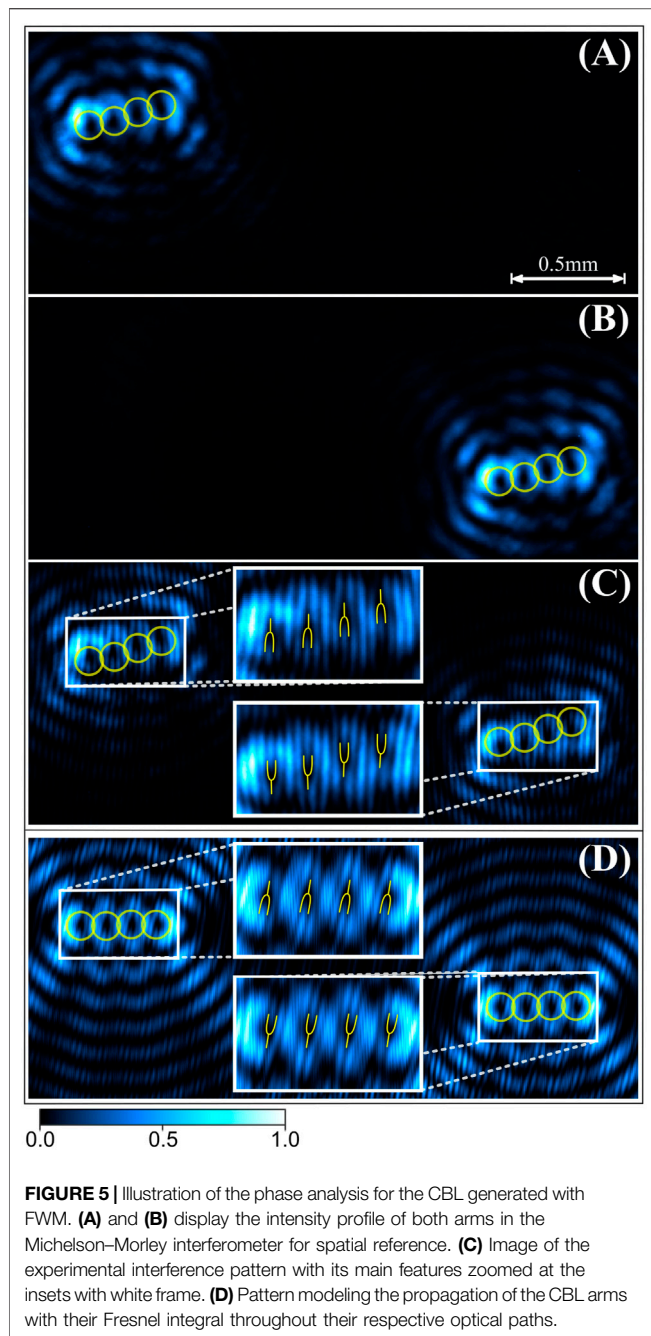


FIGURE 4 | Angular spectra of the HM-G pump beam and the CBL when Mathieu modes of order 4 were transferred from the red to the blue beam through FWM. On the left, **(A)** shows an image of HM-G taken using a CMOS camera at its Fourier plane, and on the right displays the best fit (orange) to the experimental data. The data corresponding to the CBL are depicted in **(B)**.



generate balanced images of blue rings; we observed that normal incidence of the pump beams onto the input window of the spectroscopy cell should be slightly avoided. **Figure 4B** displays a sample of the best pictures that we could achieve for CBL-Fourier rings. The best-fit parameters of its angular spectrum are shown in the third column of **Table 1**. From there, one can corroborate that $\mathcal{I}_4^{(e)} = |\mathcal{I}_4^{(o)}|$ for CBL as well. Finally, q for this measurement is equal to both the ellipticity parameter programed in the SLM and its measurement from the angular spectrum of HM-G, within the experimental accuracy.

4.2 Analysis of the CBL Phase Structure

Optical vortices were detected on CBL with the Michelson–Morley interferometer depicted in **Figure 3B** and are congruent with the expectations derived from the theory, **Figure 2**. Power and the detuning of the pump beams were kept the same as for measurements in the Fourier space. We found high-visibility interference patterns at 82°C within the experimental temperature range. **Figure 5** displays a series of images illustrating the phase analysis carried out for the example mode chosen in this article. The image of each arm serves as a spatial reference in the interference pattern. They can individually be observed by blocking its counterpart, as shown in **Figures 5A,B**. There, the yellow circles enclose zero-field regions that are candidates to host phase singularities; ideal Mathieu modes of order 4 have four vortices on their mayor axis between their foci if $\mathcal{I}_n^{(e)} = |\mathcal{I}_n^{(o)}|$, shown in **Figure 2**. This was experimentally tested on CBL by letting both arms to interfere and by modeling their propagation.

The experimental interference pattern of CBL with itself is shown in **Figure 5C**. Insets with white frames enclose two regions where inline-phase singularities are expected. Each of these areas shows four forks witnessing four optical vortices. One can observe that the absolute value of the topological charge is equal to one in all cases since the interference fringes brake into two branches. In other words, we measured $m_{CBL} = m_{HM-G}$. Therefore, even though we did not characterize the topological structure of CMW, it is theoretically expected that it does not carry any phase singularity and be Gaussian-like. Note that the forks at each arm are orientated the other way around, meaning that the rows of optical vortices imaged from each arm have opposite helicity. This is a consequence of the optical path difference traveled by each beam due to the angle θ of M1. To corroborate the physical significance of these observations, the Fresnel integral was calculated throughout the optical path of both CBL beams from their respective mirrors to the CMOS chip. Details on this model are found in [37]. **Figure 5D** is an intensity plot obtained with these calculations. Comparison between **Figures 5C,D** certifies the theoretical expectancy of the features in the CBL-phase structure that were experimentally found. The small tilt of the major axis present in Mathieu–Gauss beams [33] can also be appreciated in **Figure 5C**. It has been attributed to the Gaussian contribution required for their experimental generation [22].

5 CONCLUSION

We demonstrated that non-trivial phase structures, composed of arrays of optical vortices, are transferable through FWM in atomic gases using a ladder-type double transition—that can up- and down-convert light. This was carried out by, respectively, exciting its first and second steps with Gaussian and Mathieu–Gauss beams. We confirmed that the HM-G pump beam was appropriately characterized by the parameters of an ideal helical Mathieu mode, as well as the generated CBL, by measuring their angular spectra in their respective Fourier planes.

For probing phase singularities, we successfully introduced Michelson–Morley interferometry to the analysis of light generated by FWM in atomic gases.

Measurements in the Fourier space showed that the transverse components $\kappa_{\perp}^{G-M} \approx \kappa_{\perp}^{CBL}$. Therefore, momentum perpendicular to the propagation of helical Mathieu modes is fully transferred from HM-G to CBL as well as happens individually for the odd and even cases [26]. During the same analysis, we showed that the ellipticity parameter q of the Mathieu modes is also transferred within our experimental accuracy. With Michelson–Morley interferometry, we verified that the zero-field regions on the semi-major axis of CBL carry the optical vortices of the mode that was fed to atoms by HM-G. We also observed that the topological charge of vortices on HM-G is equal to the topological charge of vortices on CBL. This testifies that the microwave field CMW should not be carrying OAM in this very context. Nevertheless, this situation should change if the pump beam G is imprinted with phase structure as well.

Our work is a step forward to classical applications requiring multiple vortices on light with frequencies hard to achieve such as free-space multiplexing with OAM [38]. In principle, our results can be extended to generate twin beams controllably carrying multiple phase singularities. Therefore, they also contribute to enhancing OAM-multiplexing with quantum light. This exciting application has been recently demonstrated [39]. It has been subsequently employed to perform OAM quantum teleportation, tripartite entanglement, and quantum dense coding in photon pairs with similar frequencies [40, 41, 42]. Therefore, our contribution may well be the key that opens access toward implementing these applications with differently colored, quantum-correlated light carrying several OAM channels in addition to remote preparation of highly structured optical states [27].

DATA AVAILABILITY STATEMENT

The raw data supporting the conclusion of this article will be made available by the authors, without undue reservation.

REFERENCES

- Darwin CG. Notes on the Theory of Radiation. *Proc R Soc Lond A* (1932) 136: 36–52. doi:10.1098/rspa.1932.0065
- Beijersbergen MW, Allen L, van der Veen H, Woerdman JP. Astigmatic Laser Mode Converters and Transfer of Orbital Angular Momentum. *Opt Commun* (1993) 96:123–32. doi:10.1016/0030-4018(93)90535-d
- Torres PJP, Torner PL. *Twisted Photons*. Singapore: John Wiley & Sons (2011).
- Arnaut HH, Barbosa GA. Orbital and Intrinsic Angular Momentum of Single Photons and Entangled Pairs of Photons Generated by Parametric Down-Conversion. *Phys Rev Lett* (2000) 85:286–9. doi:10.1103/physrevlett.85.286
- Mair A, Vaziri A, Weihs G, Zeilinger A. Entanglement of the Orbital Angular Momentum States of Photons. *Nature* (2001) 412:313–6. doi:10.1038/35085529
- Molina-Terriza G, Torres JP, Torner L. Management of the Angular Momentum of Light: Preparation of Photons in Multidimensional Vector States of Angular Momentum. *Phys Rev Lett* (2002) 88:013601. doi:10.1103/PhysRevLett.88.013601
- Barreiro JT, Wei T-C, Kwiat PG. Beating the Channel Capacity Limit for Linear Photonic Superdense Coding. *Nat Phys* (2008) 4:282–6. doi:10.1038/nphys919
- Forbes A, Nape I. Quantum Mechanics with Patterns of Light: Progress in High Dimensional and Multidimensional Entanglement with Structured Light. *AVS Quan Sci.* (2019) 1:011701. doi:10.1116/1.5112027
- Tabosa JWR, Petrov Dv. Optical Pumping of Orbital Angular Momentum of Light in Cold Cesium Atoms. *Phys Rev Lett* (1999) 83:4967–70. doi:10.1103/physrevlett.83.4967
- Kuzmich A, Bowen WP, Boozer AD, Boca A, Chou CW, Duan L-M, et al. Generation of Nonclassical Photon Pairs for Scalable Quantum Communication with Atomic Ensembles. *Nature* (2003) 423:731–4. doi:10.1038/nature01714
- Guo J, Feng X, Yang P, Yu Z, Chen LQ, Yuan CH, et al. High-performance Raman Quantum Memory with Optimal Control in Room Temperature Atoms. *Nat Commun* (2019) 10:148–6. doi:10.1038/s41467-018-08118-5
- Zibrov AS, Lukin MD, Hollberg L, Scully MO. Efficient Frequency Up-Conversion in Resonant Coherent media. *Phys Rev A* (2002) 65. doi:10.1103/physreva.65.051801

AUTHOR CONTRIBUTIONS

LM-L built the machine, in which experiments were carried out, analyzed data, and made all the figures for this article. JA-M built experimental prototypes to implement the techniques and developed their procedures of analysis. JB-O contributed to experimental-data collection and analysis. YT demonstrated FWM for the first time in the laboratory and showed that the Michelson–Morley interferometer is a suitable tool to analyze helical Mathieu modes. NA-T brought back the apparatus to a functioning status after 1 year of null experimental work in the laboratory due the SARS-Cov-2 pandemics. RJ contributed to invaluable expertise on quasi-invariant propagation beams and developed the theory contained in this manuscript. DSS is the principal investigator of the laboratory; he designed the experimental apparatus, shaped its scientific roadmap, and supervised all the instrumental developments involved.

FUNDING

We thank the Consejo Nacional de Ciencia y Tecnología (CONACyT) for supporting through the National Laboratories Program, under Grant Nos 280181, 293471, and 299057 and through the Basic Science Grant SEP-CONACyT No. 285387. LM-L and JA-M thank CONACyT for their postgraduate study fellowships. YT thanks DGAPA-UNAM for postdoctoral support. NA-T thanks SEP-CONACyT Grant No. 285387 and CTIC for postdoctoral support. We also thank DGAPA-UNAM for constant funding through PAPIIT under Grant Nos IN108018, IN103020, and IN106821 and PFIIF-UNAM.

ACKNOWLEDGMENTS

We thank Rodrigo A. Guitierrez-Arenas for his contributions on instrumentation development for this work; Ricardo Guitierrez-Jauregui for discussions regarding this project; K. Volke-Sepulveda, Alejandro V. Arzola, and Pedro A. Quinto-Su for technical support on SLM programming.

13. Wolf J-P, Silberberg Y. Spooky Spectroscopy. *Nat Photon* (2016) 10:77–9. doi:10.1038/nphoton.2015.267
14. Lam M, Pal SB, Vogt T, Gross C, Kiffner M, Li W. Collimated UV Light Generation by Two-Photon Excitation to a Rydberg State in Rb Vapor. *Opt Lett* (2019) 44:2931. doi:10.1364/ol.44.002931
15. Downes LA, MacKellar AR, Whiting DJ, Bourgenot C, Adams CS, Weatherill KJ. Full-Field Terahertz Imaging at KiloHertz Frame Rates Using Atomic Vapor. *Phys Rev X* (2020) 10:011027. doi:10.1103/physrevx.10.011027
16. Akulshin AM, McLean RJ, Sidorov AI, Hannaford P. Coherent and Collimated Blue Light Generated by Four-Wave Mixing in Rb Vapour. *Opt Express* (2009) 17:22861–70. doi:10.1364/oe.17.022861
17. Vernier A, Franke-Arnold S, Riis E, Arnold AS. Enhanced Frequency Up-Conversion in Rb Vapor. *Opt Express* (2010) 18:17020–6. doi:10.1364/oe.18.017020
18. Offer RF, Stulga D, Riis E, Franke-Arnold S, Arnold AS. Spiral Bandwidth of Four-Wave Mixing in Rb Vapour. *Commun Phys* (2018) 1:84. doi:10.1038/s42005-018-0077-5
19. Walker G, Arnold AS, Franke-Arnold S. Trans-Spectral Orbital Angular Momentum Transfer via Four-Wave Mixing in Rb Vapor. *Phys Rev Lett* (2012) 108:243601. doi:10.1103/physrevlett.108.243601
20. Akulshin AM, Novikova I, Mikhailov EE, Suslov SA, McLean RJ. Arithmetic with Optical Topological Charges in Stepwise-Excited Rb Vapor. *Opt Lett* (2016) 41:1146. doi:10.1364/ol.41.001146
21. Chopinaud A, Jacquay M, Viaris de Lesegno B, Pruvost L. High Helicity Vortex Conversion in a Rubidium Vapor. *Phys Rev A* (2018) 97:063806. doi:10.1103/physreva.97.063806
22. Chávez-Cerda S, Padgett MJ, Allison I, New GHC, Gutiérrez-Vega JC, O’Neil AT, et al. Holographic Generation and Orbital Angular Momentum of High-Order Mathieu Beams. *J Opt B: Quan Semiclass. Opt.* (2002) 4:S52–S57. doi:10.1088/1464-4266/4/2/368
23. Durnin J, Miceli JJ, Eberly JH. Diffraction-free Beams. *Phys Rev Lett* (1987) 58:1499–501. doi:10.1103/physrevlett.58.1499
24. Dholakia K, Reece P, Gu M. Optical Micromanipulation. *Chem Soc Rev* (2008) 37:42–55. doi:10.1039/b512471a
25. Gutiérrez-López D, Maldonado-Terrón M, Hernández RJ, Vicuña-Hernández V, Ramírez-Alarcón R, Cruz-Ramírez H, et al. Spatial Control of Spontaneous Parametric Down-Conversion Photon Pairs through the Use of Apertured Bessel-Gauss Pump Beams. *Phys Rev A* (2019) 100:013802. doi:10.1103/physreva.100.013802
26. Mendoza-López LA, Acosta-Montes JG, Ángeles-Aguillón IF, Sierra-Costa D, Torres YM, Jáuregui R, et al. Generalized Angular Momentum Transfer to Up-Converted Photons via Four-Wave Mixing in Atomic Gases. *Phys Rev Res* (2021) 3:033170. doi:10.1103/physrevresearch.3.033170
27. Cameron AR, Cheng SWL, Schwarz S, Kapahi C, Sarenac D, Grabowecy M, et al. Remote State Preparation of Single-Photon Orbital-Angular-Momentum Lattices. *Phys Rev A* (2021) 104:L051701. doi:10.1103/physreva.104.l051701
28. Olver FWJ, Lozier DW, Boisvert RF, Clark CW. *The NIST Handbook of Mathematical Functions*. Cambridge, New York, Melbourne, Madrid, Cape Town, Singapore, São Paulo, Delhi, Dubai, Tokyo: Cambridge Univ. Press (2010).
29. Boyer CP, Kalnins EG, Miller W. Symmetry and Separation of Variables for the Helmholtz and Laplace Equations. *Nagoya Math J* (1976) 60:35–80. doi:10.1017/s0027763000017165
30. Rodríguez-Lara BM, Jáuregui R. Dynamical Constants for Electromagnetic fields with Elliptic-Cylindrical Symmetry. *Phys Rev A* (2008) 78:S52S57. doi:10.1103/physreva.78.033813
31. Dartora CA, Zamboni-Rached M, Nóbrega KZ, Recami E, Hernández-Figueroa HE. General Formulation for the Analysis of Scalar Diffraction-free Beams Using Angular Modulation: Mathieu and Bessel Beams. *Opt Commun* (2003) 222:75–80. doi:10.1016/s0030-4018(03)01564-5
32. Gutiérrez-Vega JC, Bandres MA. Helmholtz-Gauss Waves. *J Opt Soc Am A* (2005) 22:289–98. doi:10.1364/josaa.22.000289
33. Hernández-Hernández RJ, Terborg RA, Ricardez-Vargas I, Volke-Sepúlveda K. Experimental Generation of Mathieu-Gauss Beams with a Phase-Only Spatial Light Modulator. *Appl Opt* (2010) 49:6903. doi:10.1364/ao.49.006903
34. White AG, Smith CP, Heckenberg NR, Rubinsztein-Dunlop H, McDuff R, Weiss CO, et al. Interferometric Measurements of Phase Singularities in the Output of a Visible Laser. *J Mod Opt* (1991) 38:2531–41. doi:10.1080/09500349114552651
35. Goodman JW. Introduction to Fourier Optics. In: JW Goodman, editor. *Introduction to Fourier Optics*. 3rd ed. Englewood, CO: Roberts & Co. Publishers (2005).
36. Akulshin AM, Budker D, McLean RJ. Parametric Wave Mixing Enhanced by Velocity-Insensitive Two-Photon Excitation in Rb Vapor. *J Opt Soc Am B* (2017) 34:1016. doi:10.1364/josab.34.001016
37. Mendoza-López LA. *Análisis de luz generada via mezclado de cuatro ondas con densidad de momento angular*. Ciudad de México: Master’s thesis, Universidad Nacional Autónoma de México (2020).
38. Wang J, Yang J-Y, Fazal IM, Ahmed N, Yan Y, Huang H, et al. Terabit Free-Space Data Transmission Employing Orbital Angular Momentum Multiplexing. *Nat Photon* (2012) 6:488–96. doi:10.1038/nphoton.2012.138
39. Pan X, Yu S, Zhou Y, Zhang K, Zhang K, Lv S, et al. Orbital-Angular-Momentum Multiplexed Continuous-Variable Entanglement from Four-Wave Mixing in Hot Atomic Vapor. *Phys Rev Lett* (2019) 123:070506. doi:10.1103/physrevlett.123.070506
40. Liu S, Lou Y, Jing J. Orbital Angular Momentum Multiplexed Deterministic All-Optical Quantum Teleportation. *Nat Commun* (2020) 11:3875. doi:10.1038/s41467-020-17616-4
41. Li S, Pan X, Ren Y, Liu H, Yu S, Jing J. Deterministic Generation of Orbital-Angular-Momentum Multiplexed Tripartite Entanglement. *Phys Rev Lett* (2020) 124:083605. doi:10.1103/physrevlett.124.083605
42. Chen Y, Liu S, Lou Y, Jing J. Orbital Angular Momentum Multiplexed Quantum Dense Coding. *Phys Rev Lett* (2021) 127:093601. doi:10.1103/physrevlett.127.093601

Conflict of Interest: The authors declare that the research was conducted in the absence of any commercial or financial relationships that could be construed as a potential conflict of interest.

Publisher’s Note: All claims expressed in this article are solely those of the authors and do not necessarily represent those of their affiliated organizations, or those of the publisher, the editors, and the reviewers. Any product that may be evaluated in this article, or claim that may be made by its manufacturer, is not guaranteed or endorsed by the publisher.

Copyright © 2022 Mendoza-López, Acosta-Montes, Bernal-Orozco, Torres, Arias-Téllez, Jáuregui and Sánchez. This is an open-access article distributed under the terms of the Creative Commons Attribution License (CC BY). The use, distribution or reproduction in other forums is permitted, provided the original author(s) and the copyright owner(s) are credited and that the original publication in this journal is cited, in accordance with accepted academic practice. No use, distribution or reproduction is permitted which does not comply with these terms.